An analytic treatment of the bounded and free presheaths with arbitrary viscosity in magnetized flowing plasmas

KyuSun Chung

Citation: Phys. Plasmas 1, 2864 (1994); doi: 10.1063/1.870525
View online: http://dx.doi.org/10.1063/1.870525
View Table of Contents: http://pop.aip.org/resource/1/PHPAEN/v1/i9
Published by the American Institute of Physics.

An analytic treatment of the bounded and free presheaths with arbitrary viscosity in magnetized flowing plasmas

Kyu-Sun Chung
Department of Nuclear Engineering, Hanyang University, Seoul, South Korea

(Received 14 March 1994; accepted 2 May 1994)

Analytic solutions are derived from one-dimensional fluid equations with arbitrary shear viscosity for the free and bounded presheaths in the strongly magnetized flowing plasma. Plasma density and flow velocity are obtained analytically in terms of position along the field line, Mach number (M_∞), normalized viscosity (α), and size of bounded presheath. Simple analytic relations between the ratio (R) of sheath current and the flow Mach number [$M_\infty \equiv V_d/\sqrt{(ZT_e+T_i)/m_i}$] are derived as $R=\exp(M_\infty/M_c)$, where $M_c = 1/[1 + \sqrt{\alpha^2/1+\alpha}\arctan\sqrt{1+\alpha}]$, with less than 5% accuracy for $0\leqslant M_\infty\leqslant 0.5$. By generating two free and two bounded presheaths by two Mach probes within two free presheaths generated by a larger object than Mach probes, one can measure α and M_∞ simultaneously. The allowed range of α in terms of M_∞ is obtained, and comparisons with previous numerical analyses are also made.

I. INTRODUCTION

Although the effects of the plasma boundary have a substantial influence on the characteristics of the entire plasma in tokamaks, the physics of tokamak edge plasma is not well understood.[1] In plasma processing such as plasma etching, the mechanism between plasma and target is not well quantified in terms of plasma parameters.[2] The interaction between the Space Shuttle and the surrounding plasma in the low-Earth orbit (LEO) is still a debated problem.[3] The common features of them are (i) magnetized plasma (ion gyroradius, $\rho<$ typical object size, a) and (ii) flowing toward an object, with considering the following typical parameters: $T_e=T_i\sim 10$ eV, $B\sim 1$ T, $\rho\sim 3\times 10^{-4}$ m, a(probe)$\sim 10^{-3}$ m for hydrogen plasma in the edge of tokamak; $T_e\sim 10$ eV, $T_i\sim 1$ eV, $B\sim 0.1$ T, $\rho\sim 6\times 10^{-3}$ m, a (substrate)~ 0.1 m for argon in plasma processing; $T_e=T_i\sim 0.1$ eV, $B\sim 5\times 10^{-5}$ T, $\rho\sim 3$ m a (Space Shuttle)~ 40 m for oxygen in the ionosphere.

When the magnetic field is strong enough that the ion gyroradius is substantially smaller than an object, ion collection across the field is diffusive even if the parallel flow is dominated by inertial effects.[4] So, the quasineutral region which is called the "presheath" becomes highly elongated along the field until the cross-field diffusion is able to balance the parallel collection flow, making the presheath as effectively one dimensional. The presence of plasma flow along the field causes large asymmetries in the ion saturation current drawn to probe faces parallel and antiparallel to the magnetic field.[5,6] When using diagnostic edge probes, such flows introduce a complicating factor which must be accounted for in probe data interpretation. More importantly, the asymmetry can be used to measure the flow velocity if a reliable theory of probe operation is available.

Much effort has been devoted to measurement of the flow velocity by using two-sided directional Langmuir probes (Mach probe) in the tokamak edge or in the linear tokamak edge simulator. Mach probes have been used to measure the flow velocity in the scrape-off layer of several tokamaks,[7–10] and these measurements raise questions regarding the applicability of probe models for data interpretations. Models for probe behavior in the strongly magnetized plasma have been devoted mainly on the free presheath. Stangeby has developed one-dimensional fluid models for the measurement of parallel flow velocity by ignoring shear viscosity.[11,12] Hutchinson, however, has shown by using fluid models that shear viscosity plays an important role in determining the plasma density and flow velocity.[13,14] Chung and Hutchinson have maintained that shear viscosity should be included in analyzing magnetized presheath by kinetic analyses.[15,16] To resolve the debate in applying certain theories to analysis of probe measurement, experiments have been made in a linear machine by generating either the "free presheath,"[17] which does not contact any object along the field line, or the "bounded presheath,"[18] which does contact an object along the field line. But these experiments involve measurements fairly closed to a perturbing object and sometimes the presheath is bounded. So the relevance of the theory to current experiments is questionable, whether it is fluid,[11–14] or kinetic analyses.[15,16] Hutchinson has developed a fluid model for the bounded presheath in terms of the normalized viscosity (α: ratio of cross-field viscosity to diffusivity).[19] However, he (i) uses a numerical scheme with nonuniform meshing, (ii) assumes the variations of plasma density and flow velocity along the bounded presheath, (iii) does not mention about the upper limit of α in terms of external flow velocity, and (iv) one should assume α in order to deduce the flow velocity from his result.

It is the purpose of this work to derive analytic solutions from one-dimensional fluid equations with arbitrary shear viscosity for the free and bounded presheaths in the strongly magnetized plasma. A method to measure simultaneously the flow velocity and normalized viscosity is proposed, and the allowed range of the normalized viscosity is also obtained. Plasma density and flow velocity are calculated analytically in terms of position along the field line, external flow Mach number, normalized viscosity, and size of the bounded presheath. Section II deals with the model, governing equations. Analytic solutions for the density and flow velocity are given in the Sec. III in terms of size of bounded presheath,

 1070-664X/94/1(9)/2864/8/$6.00

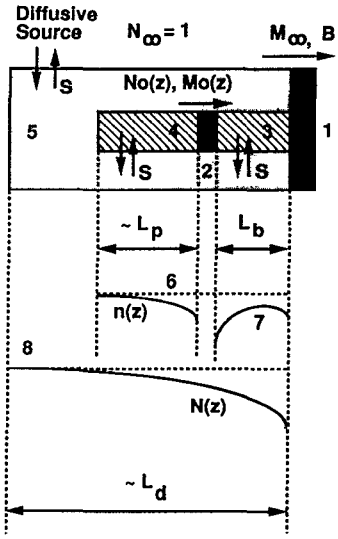

FIG. 1. Schematic diagram of a bounded and a free presheath within a free presheath of a large object: 1=Large separator for generating a free presheath; 2=small separator for generating a free and a bounded presheaths; 3=bounded presheath by small separator (downstream); 4=free presheath by small separator (upstream); 5=free presheath by large separator (upstream); and 6–8 indicate the density profiles along each presheath. a=half-size of small separator, d=half-size of large separator. "S" represents the diffusive plasma source indicating the particle and momentum exchange between outside and inside the presheath.

flow Mach number, and the normalized shear viscosity. Section IV treats a possible application to direct measurement of flow velocity and viscosity. Then, a summary of results is given in the last section.

II. MODEL

Figure 1 shows the schematic diagram of two small presheaths, one of which is bounded and the other free, within the free presheath of a large object. The density profiles (curves 6 and 8 in Fig. 1) along the free presheaths in the upstream side (regions 4 and 5) have the same shapes. Assuming the absorbing surface, plasma density decreases monotonically toward the surface of the object.[19] Along the bounded presheath (region 3), maximum density cannot exceed the reference density (n_0) and plasma contacts two surfaces (objects 1 and 2). So, the density looks like the curve 7 of Fig. 1 and this will also be shown as the curve 3 of Fig. 5. One can approximate the presheath as one dimensional and assume the electrons are governed by the Boltzmann relation for a negatively biased absorbing surface. The steady-state fluid equations for ions without volume source and collisional friction are given by

$$\nabla\cdot(n_i\mathbf{V})=0, \tag{1}$$

$$\nabla\cdot(n_i m_i\mathbf{V}\mathbf{V}+\boldsymbol{\Pi})=-\nabla P_i-Zen_i\nabla\phi, \tag{2}$$

where m_i is ion mass, n_i is ion density, P_i is ion pressure, $\mathbf{V}$ is fluid velocity, ϕ is electrostatic potential, $\boldsymbol{\Pi}$ is viscous stress, e is absolute electron charge, and Z is ion charge number. We shall assume that the phenomenological cross-field flux of ions is given by

$$n_i\mathbf{V}_\perp=-D\nabla_\perp n_i, \tag{3}$$

and the electrons are isothermal for large negative bias as

$$n_e=n_\infty\exp\left(\frac{e\phi}{T_e}\right), \tag{4}$$

where D is the anomalous cross-field diffusivity, $\perp$ means perpendicular to the magnetic field direction (z), n_e is the electron density, and n_∞ is the unperturbed plasma density.

If we focus on the parallel component of the momentum equation, treating the perpendicular diffusion equation as a source term in the parallel equations, with the following assumptions: (i) cross-field diffusivity (D) is anomalous and constant, (ii) ion temperature is constant along the presheath, (iii) parallel viscosity is neglected, and (iv) shear viscosity (η) is anomalous and given by

$$\eta=\alpha n_i m_i D,$$

where α is an arbitrary constant, then the above governing equations become

$$\frac{d(n_iV_z)}{dz}=D\nabla_\perp^2 n_i, \tag{5}$$

$$n_iV_z\left(\frac{dV_z}{dz}\right)+c_s^2\left(\frac{dn_i}{dz}\right)=D\nabla_\perp n_i\cdot\nabla_\perp V_z+\alpha D\nabla_\perp\cdot(n_i\nabla_\perp V_z), \tag{6}$$

where $c_s=[(T_i+ZT_e)/m_i]^{0.5}$ is the ion-acoustic speed. The last term of Eq. (6) is the parallel contribution of the perpendicular viscous force. In order to get simpler forms, we shall introduce nondimensional variables and approximations in the cross-field direction including

$$n=\frac{n_i}{n_\infty},\quad M=\frac{V_z}{c_s},\quad y=\frac{z}{L_p}=\frac{zD}{a^2c_s},$$

$$\nabla_\perp Q\approx(Q_\infty-Q)/a,\quad \nabla_\perp^2 Q\approx(Q_\infty-Q)/a^2,$$

where Q is a general parameter for density and flow velocity, a is the half-size of a perturbing object, and L_p is the characteristic length of the presheath.

Approximation and nondimensionalization can be done the same as in Hutchinson's case.[19] In making approximations, however, he chose the parallel contribution of the perpendicular viscous force [the last term of Eq. (6)] as

$$\alpha D\nabla_\perp\cdot(n_i\nabla_\perp V_z)\approx\alpha Dn_i\frac{(V_\infty-V_z)}{a^2} \tag{7}$$

by saying that he "has ignored the spatial dependence of viscosity." However, he just ignored the spatial dependence of shear viscosity (η) on the ion density (n_i) in the cross-field direction (r) not in the parallel direction (z) along the presheath, because density variation $n_i(z)$ across the flux tube can exist, and η depends upon $n_i(z)$. In addition, since the approximation of Eq. (7) is just one type of approximation and there is no unique procedure for this, we could just as well make it

$$\alpha D\nabla_\perp\cdot(n_i\nabla_\perp V_z)\approx\alpha D(n_\infty-n_i)\frac{(V_\infty-V_z)}{a^2}, \tag{8}$$

and it allows us to get analytic solutions of density and flow velocity for an arbitrary α. With nondimensional variables and approximation of Eq. (8), Eqs. (5) and (6) become

$$\frac{d(nM)}{dy}=(1-n), \tag{9}$$

$$nM\left(\frac{dM}{dy}\right)+\frac{dn}{dy}=(1+\alpha)(1-n)(M_\infty-M). \tag{10}$$

Rearrangement of these equations produces the following equations:

$$\frac{dn}{dy}=(1-n)\frac{[(1+\alpha)M_\infty-(2+\alpha)M]}{(1-M^2)}, \tag{11}$$

$$\frac{dM}{dy}=\frac{(1-n)}{n}\frac{[1-(1+\alpha)M_\infty M+(1+\alpha)M^2]}{(1-M^2)}. \tag{12}$$

III. ANALYTIC SOLUTIONS

Dividing Eq. (11) by Eq. (12) results in

$$\frac{dn}{dM}=\frac{n[-(2+\alpha)M+(1+\alpha)M_\infty]}{1-(1+\alpha)M_\infty M+(1+\alpha)M^2}. \tag{13}$$

Rearrangement for the direct integration of Eq. (13) produces

$$\int_{n_\infty}^{n}\frac{dn}{n}=\int_{M_\infty}^{M}dM\,\frac{-(2+\alpha)M+(1+\alpha)M_\infty}{1-(1+\alpha)M_\infty+(1+\alpha)M^2}, \tag{14}$$

where n_∞ and M_∞ are the normalized unperturbed plasma density and flow Mach number outside the free presheath. From this the following solution for plasma density is obtained:

$$n(M)=[(1+\alpha)M^2-(1+\alpha)M_\infty M+1]^{-\delta}\times\exp\left\{\frac{\alpha M_\infty}{\sqrt{q}}\left[\arctan\left(\frac{(1+\alpha)(2M-M_\infty)}{\sqrt{q}}\right)-\arctan\left(\frac{(1+\alpha)M_\infty}{\sqrt{q}}\right)\right]\right\}, \tag{15}$$

where $\delta=(2+\alpha)/(2+2\alpha)$ and $q=4(1+\alpha)-(1+\alpha)^2M_\infty^2$. If we check the validity of Eq. (15), then $n(M=M_\infty)=1$, which represents the unperturbed density, and $n(M=1,\ \alpha=0)=1/(2-M_\infty)$, which is the exactly same form as Stangeby's result.[12]

In order for $n(M)$ to be real, q should be positive, i.e.,

$$q=4(1+\alpha)-(1+\alpha)^2M_\infty^2>0,$$

and Fig. 2 shows the relation of the normalized viscosity (α) to the external flow velocity (M_∞). Although α is an arbitrary number, it has an allowed range in terms of plasma flow velocity, e.g., $0\leq\alpha\leq3$ for $M_\infty=1$. For positive viscosity, plasma flow velocity cannot exceed Mach number 2 [$V_d=2\sqrt{(ZT_e+T_i)/m_i}$]. For ultrasupersonic flow ($M_\infty>2$), there is the possibility that viscosity could be negative, although the possible physical meaning of this is not clear, yet.

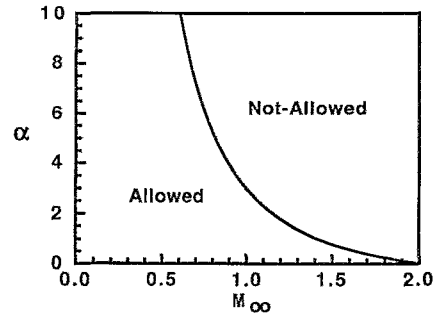

FIG. 2. Allowed range of the normalized viscosity (α) in terms of the external flow velocity (M_∞). α can be negative for $M_\infty>2$.

A. Free presheath

From Eq. (15) the sheath density is given by

$$n_s\equiv n(M=1)=[(2+\alpha)-(1+\alpha)M_\infty]^{-\delta}\times\exp\left\{\frac{\alpha M_\infty}{\sqrt{q}}\left[\arctan\left(\frac{(1+\alpha)(2-M_\infty)}{\sqrt{q}}\right)-\arctan\left(\frac{(1+\alpha)M_\infty}{\sqrt{q}}\right)\right]\right\}, \tag{16}$$

Figure 3 shows the sheath density in terms of α for $-1\leq M_\infty\leq1$. The present model produces larger values than the numerical fluid model of Hutchinson,[19] while the kinetic model of Chung[15] produces smaller values for $M_\infty<0$ (downstream) and larger for $M_\infty>0$ (upstream). From Eq. (16) the ratio of up- to downsheath current densities is calculated as

$$R(M_\infty)\equiv\frac{n_s(M_\infty>0)}{n_s(M_\infty<0)}=\left(\frac{(2+\alpha)+(1+\alpha)M_\infty}{(2+\alpha)-(1+\alpha)M_\infty}\right)^{\delta}\times\exp\left[\frac{\alpha M_\infty}{\sqrt{q}}\left(\arctan\frac{(1+\alpha)(2-M_\infty)}{\sqrt{q}}+\arctan\frac{(1+\alpha)(2+M_\infty)}{\sqrt{q}}\right)\right], \tag{17}$$

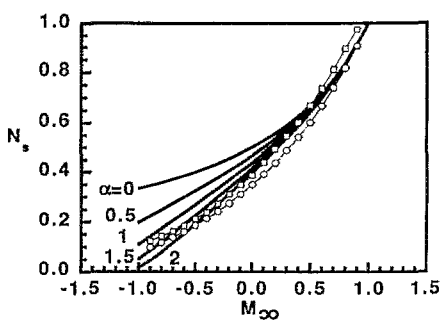

FIG. 3. Sheath density in terms of α for $-1\leq M_\infty\leq1$. Open squares are from kinetic analysis with $\alpha=1$,[15] and open circles are from fluid analysis.[13]

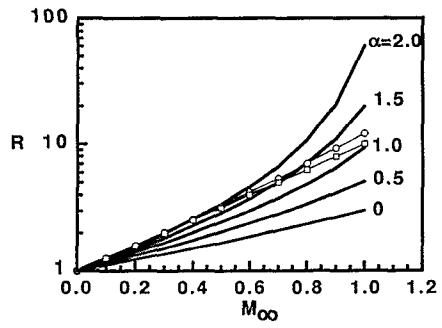

FIG. 4. Ratio of current densities in terms of α for $-1 \leqslant M_\infty \leqslant 1$. Numerical results of one-dimensional fluid (open circle)[13] and kinetic models (open square)[15] are also included for $\alpha=1$.

and Fig. 4 shows the ratio of current densities. Numerical results of one-dimensional fluid and kinetic models are also included for $\alpha=1$. Present analytic treatment produces smaller ratios than numerical fluid and kinetic models. For nonviscous flow ($\alpha=0$) with $M_\infty=1$, the ratio (R) becomes 3, and for the strongly viscous case ($\alpha=1$), this gives 9.3, while Hutchinson's produces 12. Hence, the ratio of two cases is 3.1 instead of 4 as Hutchinson found.[14]

Since there has been discussion of the flow reversal or flow drift near the reconnection point of magnetic field in the divertor tokamak,[20] and it may be small Mach number, then it might be useful to derive a simple formula for small Mach number. For $0<M_\infty \ll 1$, Eq. (16) is approximated as

$$R(M_\infty) \approx \left(1+\frac{(1+\alpha)M_\infty}{(2+\alpha)}\right)^{2\delta} \exp\left(\frac{\alpha M_\infty \arctan\sqrt{1+\alpha}}{\sqrt{1+\alpha}}\right).$$

By taking the logarithm of the above equation, and using the Taylor expansion of $\ln[1+x]$ for $|x|<1$, it can be further reduced as

$$R \approx \exp(M_\infty/M_c), \tag{18}$$

where M_c is the calibration factor:

$$M_c=\left(1+\sqrt{\frac{\alpha^2}{1+\alpha}}\arctan\sqrt{1+\alpha}\right)^{-1}.$$

This recovers the simple exponential form as in other models.[7,15,16] The maximum difference between Eqs. (17) and (18) is less than 5% for $0 \leqslant M_\infty \leqslant 0.5$.

B. Bounded presheath

If one applies the above theory to the bounded presheath, one can analytically obtain the normalized density (n) and the flow Mach number (M) along the presheath in terms of the flow Mach number (M_0) outside the bounded presheath, normalized viscosity (α), and size of the bounded presheath (L_b). For the analysis of the bounded presheath with plasma flow, let us define n_0, M_0, and n_{m0} as density, flow Mach number outside the bounded presheath, and the maximum density along the presheath for $M_0=0$, respectively. As M_0 gets bigger, there is a region where the density $[n(z)]$ along the bounded presheath becomes larger than n_{m0}. So, the maximum density along the bounded presheath has the value between n_{m0} and n_0, while $-1 \leqslant M \leqslant 1$. Then one can always find a position z_0 at which the reference velocity M_0 is defined as $M_0 \equiv M$ $(z=z_0)$ along the bounded presheath $(0<z_0<L_b)$, and the reference density $n_m \equiv n(z=z_0)$. Hutchinson assumes the spatial variations of the density and the flow velocity with nonuniform meshing, and separates the bounded presheath into two regions, i.e., $0 \leqslant z \leqslant z_0$ and $z_0 \leqslant z \leqslant L_b$ (in his paper he uses z_m instead of z_0) or $-1 \leqslant M \leqslant M_0$ and $M_0 < M \leqslant +1$.[19] Then he numerically integrates Eq. (13) for these regions, with a slightly different form due to different approximation to obtain the density. However, without this complicated procedure, in order to obtain the density along the bounded presheath, one simply needs to replace the lower bound limits of Eq. (14), i.e., $n_\infty \to n_m$, $M_\infty \to M_0$:

$$n(M)=n_m[(1+\alpha)M^2-(1+\alpha)M_0M+1]^{-\delta} \times \exp\left\{\frac{\alpha M_0}{\sqrt{q}}\left[\arctan\left(\frac{(1+\alpha)(2M-M_0)}{\sqrt{q}}\right)-\arctan\left(\frac{(1+\alpha)M_0}{\sqrt{q}}\right)\right]\right\}, \tag{19}$$

where $-1 \leqslant M_0 \leqslant +1$ and $q=4(1+\alpha)-(1+\alpha)^2M_0^2$. Putting Eq. (19) into Eq. (12) by replacing M_∞ with M_0 leads to the following equation:

$$\frac{dM}{dy}=\frac{1-n_mG(M)^{-\delta}\exp[H(M)]}{n_mG(M)^{-\delta}\exp[H(M)]}\frac{G(M)}{(1-M^2)}, \tag{20}$$

where

$$G(M) \equiv 1-(1+\alpha)M_0M+(1+\alpha)M^2$$

and

$$H(M) \equiv (\alpha M_0/\sqrt{q})\{\arctan[(1+\alpha)(2M-M_0)/\sqrt{q}] - \arctan[(1+\alpha)M_0/\sqrt{q}]\}.$$

Then the position along the bounded presheath is obtained as

$$y(M)=\int_1^{M_0}\frac{n_mG(M)^{-\delta}\exp[H(M)]}{1-n_mG(M)^{-\delta}\exp[H(M)]}\frac{1-M^2}{G(M)}\,dM, \tag{21}$$

where $-1 \leqslant M_0 \leqslant +1$. Since the integrand of Eq. (21) is an explicit equation of M, $y(M)$ can be obtained explicitly in terms of M_0 and n_m. From this one can obtain the flow velocity $M(y)$ in terms of normalized position y, and density is also obtained by inserting $M(y)$ into Eq. (19).

Figure 5 shows the variations of density and flow velocity. Both cases show the variations with different flow velocity (M_0) outside of the bounded presheath within the free presheath. A reference case is chosen for $n_m=0.7$, $\alpha=1$, and $M_0=0$. When there is no flow outside the bounded presheath, the shape of density variation along the field line is symmetric and maximum density is less than that outside the free presheath (curve 1), while the flow velocity (M) varies between -1 and $+1$ (curve 4). Emmert *et al.* solved this problem by putting $n_0=1$=maximum density by assuming that the plasma parameters are symmetric when there is no plasma flow ($M_0=0$).[21] If there is flow, symmetries in den-

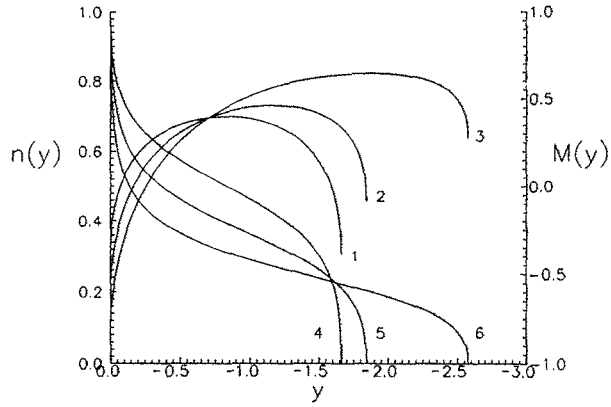

FIG. 5. Variations of the flow velocity (curves 1–3) and density (curves 4–6) along the bounded presheath with different flow velocities [M_0=0 (curves 1 and 4),=0.5 (curves 2 and 5), and=0.9 (curves 3 and 6)] outside of the bounded presheath within the free presheath. Reference case is chosen as n_m=0.7 for M_0=0.

sity and velocity variations are broken [curves 2 (M_0=0.5) and 3 (M_0=0.9) for density, and curves 5 (M_0=0.5) and 6 (M_0=0.9) for velocity]. The present analytic treatment produces slightly larger density, velocity, and the size of the bounded presheath than those of Hutchinson's numerical method.[19]

The sheath density at the surface of a small object within a large object is calculated by putting M=1 in Eq. (19). Figure 6 shows the sheath density in terms of size of bounded presheath (total connection length between the two boundaries) with different normalized viscosity ($0 \leq \alpha \leq 2$) for the M_0=0.5 (upstream: curves 1–5) and M_0=−0.5 (downstream: curves 6–10) cases. The sheath density gets smaller with α for the downstream (M_0<0) case, while it increases

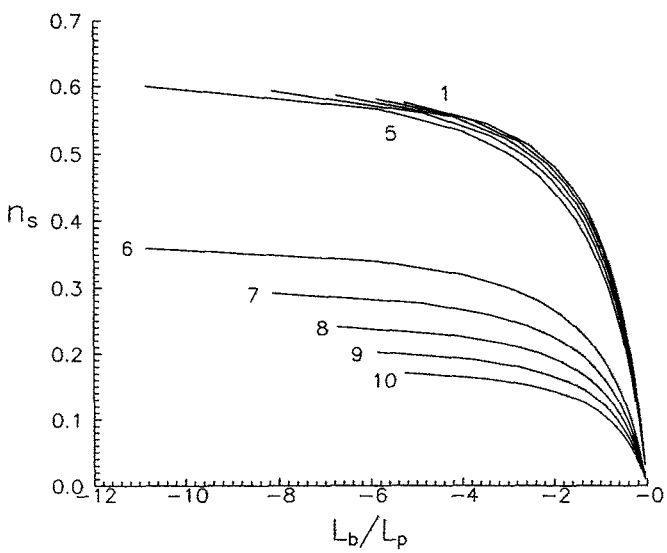

FIG. 6. Sheath density in terms of size of bounded presheath (total connection length between the two boundaries) with different α for M_∞=0.5 (upstream: curves 1–5) and M_∞=−0.5 (downstream: curves 6–10). α is 0.0 for curves 5 and 6, 0.5 for curves 4 and 7, 1.0 for curves 3 and 8, 1.5 for curves 2 and 9, and 2.0 for curves 1 and 10.

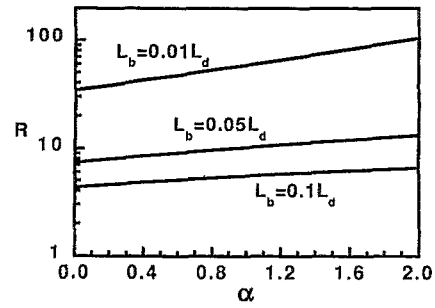

FIG. 7. Current ratios (R) with the normalized viscosity (α) and the size (L_b) of the bounded presheath (L_b=0.01, 0.05, 0.1L_d) for n_∞=1 and M_∞=0.

with α for the upstream (M_0>0) case. The change is more drastic for the downstream case than the upstream case. This implies that the sheath density is more affected by the size of the bounded presheath when the external flow is away from the probe (downstream) than it is toward the probe (upstream) due to the imposed condition of flow velocity $|M|$=1 at the boundary.

When n_0 and M_0 are varying along the free presheath due to a large object, $n_0(L_b)$ and $M_0(L_b)$ should be used for the calculation of the density [$n(z)$], flow velocity [$M(z)$] along the bounded presheath, and ratio of the sheath densities at each L_b, where L_b is the position of the small object ("2" in Fig. 1) along the free presheath by the large object ("1" in Fig. 1), i.e., the size of the bounded presheath. Figure 7 shows the current ratios (R) in terms of the normalized viscosity (α) with various sizes (L_b) of the bounded presheath for n_∞=1 and M_∞=0 (no drift outside the large separator). Here R gets bigger with larger α and with smaller L_b, but L_b has a stronger effect on R than α in the bounded presheath. Since the slope of R in terms of α, $dR/d\alpha$, become steeper as L_b gets smaller, the difference in asymptotic values of R between for α=0 and for α=1 becomes larger, i.e., they do not converge on each other as L_b gets smaller. Therefore, information in the measurement of R is not lost as L_b gets smaller.

Comparisons of ours with Hutchinson's[19] for density and flow velocity along the bounded presheath are shown in Fig. 8(a), and the ratios of current densities in Fig. 8(b). These are made for α=1, n_∞=1, and M_∞=0 of the large free presheath. Present analytic results give larger density [$n_0(z)$] and smaller velocity [$M_0(z)$] than those of Hutchinson[19] along the free presheath of the large separator. This affects the ion collection toward each surface of the small separator. The difference in ratios (R) of sheath current densities collected by two opposite sides of the small separator gets bigger as the ratio of size of small probe separator to large [$L \equiv (a/d)^2$] gets larger, and the biggest difference is about 17% between the two approximations. The present analytic model produces smaller ratios of the sheath current densities than those of the numerical method.[19] The differences between ours and Hutchinson's are the following: (i) viscosity term is approximated differently; (ii) $n_0(L_b)$ and $M_0(L_b)$ are obtained analytically in ours, while they are assumed in his;

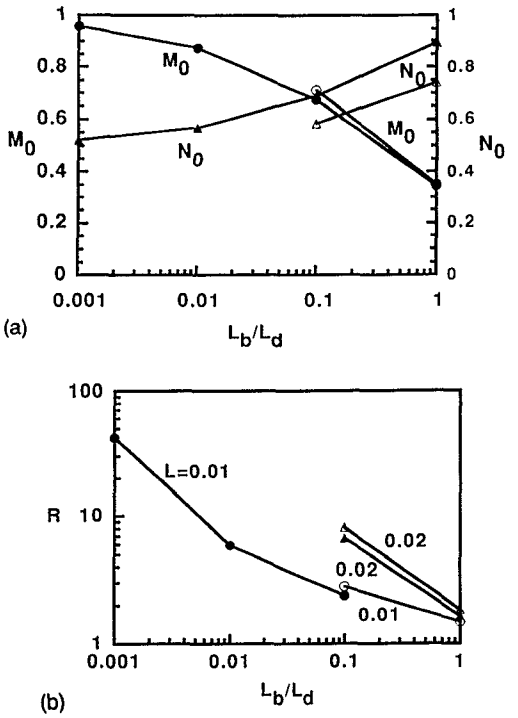

FIG. 8. (a) Variations of density (solid triangle) and flow velocity (solid circle) outside of the bounded presheath within the free presheath by a large separator. (b) Ratios of current densities for $L \equiv (a/d)^2 = 0.01$ (solid circle) and 0.02 (solid triangle). These are made for $n_\infty = 1$ and $M_\infty = 0$ outside of the large free presheath. Open legends are from numerical model of Hutchinson.[19]

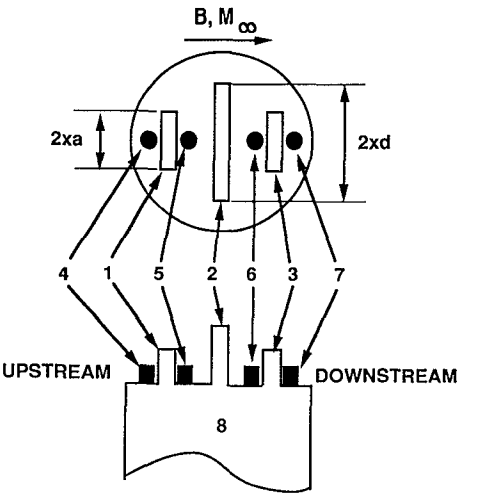

FIG. 9. Direct visco-Mach probe (DVMP) which generates six presheaths, four are free and other two are bounded presheaths. a is the half-size of the small separator (1 and 3: SS), and d is that of the large separator (2: LS). 4=Probe collecting upstream ion current in a small free presheath by SS(1) within a large free presheath formed upstream side of LS. 5=Probe collecting downstream ion current in a bounded presheath by SS(1) and LS within a large free presheath formed upstream side of LS. 6=Probe collecting downstream ion current in a bounded presheath by SS(3) and LS within a large free presheath formed downstream side of LS. 7=Probe collecting upstream ion current in a small free presheath by SS(3) within a large free presheath formed downstream side of LS. 8=Probe holder.

and (iii) $n(z)$ and $M(z)$ are calculated along the bounded presheath by direct integration for $0 < n_m < n_0(L_b)$ in ours, while Hutchinson obtained these by numerical analysis of Eqs. (9) and (10) with nonuniform meshing by Patankar's numerical methods.[22] [Note: n_m is the density at $M(z) = M_0(L_b)$ along the bounded presheath.]

IV. APPLICATIONS

By generating two free presheaths and two bounded presheaths by two Mach probes within two free presheaths generated by a large object, one can measure α and M_∞ simultaneously deduced from the measurement of R_u by one Mach probe located in the upstream side of the large object, and R_d by the other Mach probe in the downstream side.

A. Visco-Mach probe with direct scheme

We will consider a probe system as in Fig. 9, which generates four free and two bounded presheaths: two small separators (SS) "1" and "3" generate two free presheaths in the upstream side and two bounded in the downstream side; a large separator (LS) "2" generates two free presheaths in both directions. This probe system is composed of two Mach probes, one near probes "4" and "5" measures the ratio $(R_u = J_4/J_5)$ of ion saturation currents collected in the upstream side of the free presheath generated by the large separator, and the other near probes "6" and "7" takes the ratio $(R_d = J_7/J_6)$ of currents collected in the downstream side. Each Mach probe has two different presheaths; one is the free presheath and the other is bounded. If we assume the same transport coefficients in these six presheaths and the plasma around them, we can simultaneously deduce the normalized viscosity $(\alpha \equiv \eta/n_i m_i D)$ and the plasma flow velocity (M_∞) without any numerical iteration. Let us call this probe a "direct-visco-Mach probe (DVMP)."

Figure 10 shows the ratio (R) of sheath current densities by a Mach probe (MP) versus α in terms of M_∞ outside of the presheath generated by LS and a fixed position

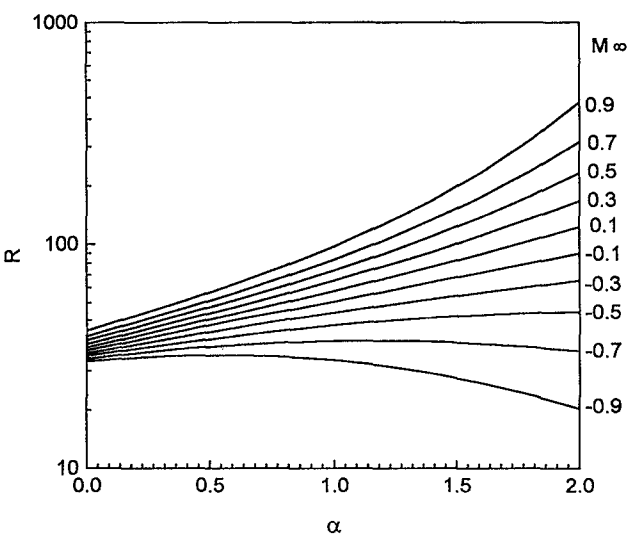

FIG. 10. Ratio (R) of sheath current densities by a Mach probe (MP) versus α in terms of M_∞ outside of the free presheath generated by a large separator (LS), and a fixed position $(L_b = 0.1 L_d)$ of MP within a free presheath by LS with a fixed ratio $[L \equiv (a/d)^2 = 0.01]$ of probe separators.

$(L_b=0.1L_d)$ of MP within a free presheath by LS with a fixed ratio $[L\equiv(a/d)^2=0.01]$ of probe separators. By using this figure we can deduce α and M_∞ simultaneously from measurement of R_u and R_d by the following: one Mach probe in the upstream side ($M_\infty>0$) takes the ratio (R_u) of currents of free and bounded presheaths generated by SS ("1") within the free presheath of LS ("2"); and the other MP in the downstream side ($M_\infty<0$) takes the ratio (R_d). If we measure the ratios as $R_u=J_4/J_5=60$, $R_d=J_7/J_6=35$, then we can deduce α as 0.61 and M_∞ as 0.7 by the following procedures: For $M_\infty=0$, $\alpha(R_u=60)=1.2$, and $\alpha(R_d=35)=0.15$. Two values of α do not coincide: $\alpha(R_{s1}=60)=0.8$ for $M_\infty=0.5$, and $\alpha(R_{s2}=35)=0.4$ for $M_\infty=-0.5$. Two values of α do not coincide either. But in this case they get closer: $\alpha(R_{s1}=60)=0.5$ for $M_\infty=0.9$, and $\alpha(R_{s2}=35)$ cannot be found for $M_\infty=-0.9$. For $|M_\infty|=0.9$, there is no way to find α. From this information we know that α is to be found between the $|M_\infty|=0.9$ and $|M_\infty|=0.5$ lines. By making detailed lines between the $|M_\infty|=0.9$ and $|M_\infty|=0.5$ lines, we can find $\alpha=0.61$ and $M_\infty=0.7$ simultaneously.

B. Error analysis

In any real experiment there are errors in the measured quantities. It is therefore important to ask how sensitive our determination of M_∞ and α is to uncertainties in R_u and R_d. Let us define parameters as the following: $\sigma\equiv$error, $j\equiv$ion sheath current density, $u\equiv$upstream, $d\equiv$downstream, $r\equiv$current density ratio, $\alpha\equiv$normalized viscosity, $m\equiv$Mach number, then the error σ_{ru} of the ratio $R_u\equiv J_{uu}/J_{ud}$ and σ_{rd} of R_d are given by

$$\frac{\sigma_{ru}}{R_u}=\left(\frac{\sigma_{juu}^2}{J_{uu}^2}+\frac{\sigma_{jud}^2}{J_{ud}^2}\right)^{0.5},\quad \frac{\sigma_{rd}}{R_d}=\left(\frac{\sigma_{jdu}^2}{J_{du}^2}+\frac{\sigma_{jdd}^2}{J_{dd}^2}\right)^{0.5},$$

when J_{uu}, J_{ud}, J_{du}, and J_{dd} are uncorrelated.[23] Since the normalized viscosity α and flow Mach number M_∞ are not explicit functions of the ratios R_u and R_d, and are simultaneously determined by them, the errors in α and M_∞ cannot be easily calculated. One possible way is to take same relative error as those of R_u and R_d, i.e., if $\sigma_{ru}/R_u=10\%=\sigma_{rd}/R_d$, then $\sigma_\alpha/\alpha=10\%=\sigma_m/M_\infty$. So, for $R_u=60\pm6$, $R_d=35\pm3.5$, then $\alpha=0.61\pm0.06$, $M_\infty=0.7\pm0.07$.

The other way to determine the error in α and M_∞ is to use the current ratio by the large separator, i.e., to use the following relation:

$$M_\infty=M_c\ \ln[R_\infty]=M_c\ \ln[J_4/J_7].$$

Since the calibration factor M_c is a function of α as in Eq. (18), the error σ_m of M_∞ can be calculated by

$$\begin{aligned}M_\infty+\sigma_m&=M_c(\alpha+\sigma_\alpha)\ln[R_\infty+\sigma_{r\infty}]\\&\approx\left(M_c(\alpha)+\sigma_\alpha\left|\frac{dM_c}{d\alpha}\right|\right)\left(\ln[R_\infty]+\frac{\sigma_{r\infty}}{R_\infty}\right)\\&\approx M_c(\alpha)\ln[R_\infty]+\sigma_\alpha\left|\frac{dM_c}{d\alpha}\right|\ln[R_\infty]\\&\quad+\frac{\sigma_{r\infty}}{R_\infty}M_c(\alpha).\end{aligned}$$

So the error σ_m of Mach number M_∞ is obtained

$$\sigma_m\approx\sigma_\alpha\left|\frac{dM_c}{d\alpha}\right|\ln[R_\infty]+\frac{\sigma_{r\infty}}{R_\infty}M_c(\alpha),$$

if σ_α is predetermined. For example, if $\sigma_{r\infty}/R_\infty=10\%$, $\sigma_\alpha=0.06$, and $R_u=60$, $R_d=35$ and $R_\infty=3$, then $\sigma_m=(0.06)(|-0.76|)(\ln[3])+(0.1)(0.64)=0.11$. Hence, the flow Mach number $M=0.7\pm0.11$. Therefore, the error in measuring M_∞ is about 15%.

V. CONCLUSIONS

Theories of the free and bounded presheaths are treated analytically by using one-dimensional fluid approximations. Plasma density and flow velocity are calculated analytically in terms of position along the field line, Mach number (M_∞), normalized viscosity (α), and size of bounded presheath (L_b). A simple analytic relation between the ratio (R) of sheath current and the flow Mach number $[M_\infty\equiv V_d/\sqrt{(ZT_e+T_i)/m_i}]$ are obtained as $R=\exp(M_\infty/M_c)$, where $M_c=1/(1+\sqrt{\alpha^2/1+\alpha}\arctan\sqrt{1+\alpha})$, with less than 5% accuracy for $0\leq M_\infty\leq0.5$. Maximum difference between flow velocity deduced by analytic treatment and that by the numerical one is about 17% for $0\leq\alpha\leq1$. Present one-dimensional results can be used for modeling the scrape-off layer in the tokamak edge and plasma processing with inclusion of diffusive source and viscosity, although it needs to be verified by two-dimensional calculation with additional factors such as ionization, charge exchange, and spatial variation of temperature, diffusivity, and magnetic field. Even when probes are close to other structures, present solutions allow quantitative analysis of not only the operation of simple electric probes but also simultaneous measurement of the α and M_∞ by using a relation of the current density ratio to L_b, α, and M_∞. A "visco-Mach" probe with a direct scheme is proposed to measure them simultaneously by generating two free and two bounded presheaths by two Mach probes within the free presheaths at a larger object than Mach probes. Allowed range of α is given in terms of M_∞. For instance, $0\leq\alpha\leq3$ for $M_\infty=1$.

[1]P. C. Stangeby and G. M. McCracken, Nucl. Fusion **30**, 1225 (1990).
[2]H. V. Boenig, *Fundamentals of Plasma Chemistry and Technology* (Technomic, Lancaster, PA, 1988).
[3]See National Technical Information Document No. 87N20055 [U. Samir, in Space Technology Plasmas Issue in 2001, edited by H. Garrett, J. Feynman, and S. Gabriel (JPL, Caltech., 1986), p. 69]. Copies may be ordered from NTIS Springfield, Virginia 22161.
[4]I. H. Hutchinson, *Principles of Plasma Diagnostics* (Cambridge University Press, New York, 1987), Chap. 3.

[5]G. Proudfoot, P. J. Harbour, J. Allen, and A. Lewis, J. Nucl. Mater. **128–129**, 180 (1984).
[6]A. S. Wan, B. LaBombard, B. Lipschultz, and T. F. Yang, J. Nucl. Mater. **145–147**, 191 (1987).
[7]P. J. Harbour and G. Proudfoot, J. Nucl. Mater. **121**, 222 (1984).
[8]J. Allen and P. J. Harbour, J. Nucl. Mater. **145–147**, 264 (1987).
[9]M. Laux, H. Grothe, K. Guenther, A. Herrmann, D. Hildebrandt, P. Pech, H.-D. Reiner, H. Wolff, and G. Ziegenhagen, J. Nucl. Mater. **162–164**, 200 (1989).
[10]C. S. MacLatchy, C. Boucher, D. A. Poirier, and J. Gunn, Rev. Sci. Instrum. **63**, 3923 (1992).
[11]P. C. Stangeby, J. Phys. D: Appl. Phys. **15**, 1007 (1982).
[12]P. C. Stangeby, Phys. Fluids **27**, 2699 (1984).
[13]I. H. Hutchinson, Phys. Fluids **30**, 3777 (1987).
[14]I. H. Hutchinson, Phys. Rev. A **37**, 4358 (1988).
[15]K.-S. Chung and I. H. Hutchinson, Phys. Rev. A **38**, 4721 (1988).
[16]K.-S. Chung and I. H. Hutchinson, Phys. Fluids B **3**, 3053 (1991).
[17]K.-S. Chung, I. H. Hutchinson, B. LaBombard, and R. W. Conn, Phys. Fluids B **1**, 2229 (1989).
[18]B. LaBombard, R. W. Conn, Y. Hirooka, R. Lehmer, W. K. Leung, R. E. Nygren, Y. Ra, G. Tynan, and K.-S. Chung, J. Nucl. Mater. **162–164**, 314 (1989).
[19]I. H. Hutchinson, Phys. Fluids B **3**, 847 (1991).
[20]S. I. Krasheninnikov, Nucl. Fusion **32**, 1927 (1992).
[21]G. A. Emmert, R. M. Wieland, A. T. Mense, and J. N. Davidson, Phys. Fluids **23**, 803 (1980).
[22]S. V. Patankar, *Numerical Heat Transfer and Fluid Flow* (Hemisphere, New York, 1980).
[23]P. R. Bevington and D. K. Robinson, *Data Reduction and Error Analysis for the Physical Sciences*, 2nd ed. (McGraw-Hill, New York, 1992).